Resistance of group III nitrides irradiated with a 10 keV electron beam; comparison of the cathodoluminescence emission of GaN quantum dots, quantum wells and (Al)GaN epitaxial layers

2006 J. Phys.: Condens. Matter 18 1033

(http://iopscience.iop.org/0953-8984/18/3/019)

INSTITUTE OF PHYSICS PUBLISHING JOURNAL OF PHYSICS: CONDENSED MATTER

J. Phys.: Condens. Matter **18** (2006) 1033–1049 doi:10.1088/0953-8984/18/3/019

Resistance of group III nitrides irradiated with a 10 keV electron beam; comparison of the cathodoluminescence emission of GaN quantum dots, quantum wells and (Al)GaN epitaxial layers

B Sieber

Laboratoire de Structure et Propriétés de l'Etat Solide, UMR CNRS 8008, Bâtiment C6
Université des Sciences et Technologies de Lille, 59655 Villeneuve d'Ascq Cédex, France

E-mail: Brigitte.Sieber@univ-lille1.fr

Received 22 July 2005, in final form 18 November 2005
Published 6 January 2006
Online at stacks.iop.org/JPhysCM/18/1033

Abstract

We present a comparative study of the *in situ* modifications induced by a 10 keV electron beam in gallium nitride (GaN) quantum wells and quantum dots as well as in ELOG (epitaxial laterally overgrown GaN) and AlGaN epilayers. Cathodoluminescence (CL) experiments were performed to investigate the room temperature evolution of the optical properties as a function of the beam current density. Higher dot resistance is much more apparent when the beam current density is larger than about 6 A cm^{-2}. Recombination enhanced diffusion of defects is involved in the degradation of the CL signal. The two serial mechanisms inferred to be present in the degradation process are described.

(Some figures in this article are in colour only in the electronic version)

1. Introduction

Group III nitride semiconductors are currently the most promising candidates for the fabrication of blue and ultra-violet (UV) laser diodes [1]. However these devices require long-lasting stability of their optical properties under electron or photon injection. In this respect, quantum dots (QDs) seem to be well suited thanks to the large confinement of charge carriers as compared with that provided by quantum wells and epilayers [2]. The strong spatial localization of carriers in QDs leads to a reduced efficiency of non-radiative (NR) recombinations which are thought to lie at the origin of the luminescence intensity degradation [3–5]. Several research works have shown that this was indeed the case when the dots were irradiated with either protons or electrons. A large increase in the radiation resistance of QDs has been already evidenced in the case of irradiation of III arsenide with high energy electrons [6], protons [7–9], high

and low energy ions [10, 11], as well as II–VI QDs irradiated with photons [12, 13], and electrons [13]. Even stability over 450 h of a long wavelength QD laser made on a GaAs substrate was reported [14]. But recent investigations have shown that the luminescence of gallium nitride (GaN) QDs can be definitely degraded by a 10 keV electron beam (e-beam) injection [15, 16]. It was shown that the degradation rate was slowed down by increasing the injected e-beam current density. The saturation of non-radiative (NR) centres at the injection point could properly explain this result [16].

In the present paper we address the question of the specificity of the time evolution of the QD optical properties under e-beam injection as compared with those of quantum wells (QWs) and epilayers. For that purpose, their room temperature optical properties are recorded as a function of the injection time by means of cathodoluminescence (CL) experiments. Special attention is paid to the influence of the current density of the low energy (10 keV) e-beam. We compare the irradiation resistance of heterostructures containing QDs, QWs and AlGaN barriers together with that of a thick epitaxial laterally overgrown GaN (ELOG) epilayer.

2. Experimental details

The first nitride-based heterostructure (figure 1) studied in this work is one with a graded index separate confinement heterostructure (SCH–QD). It has been grown at 730 °C by plasma assisted molecular beam epitaxy on a 6H (0001)-SiC substrate [18].

A 1 μm AlN epilayer was first deposited on the substrate. The SCH region consisted of five layers of GaN QDs embedded in 15 nm $Al_{0.27}Ga_{0.73}N$ cladding layers deposited between two 45 nm $Al_{0.27}Ga_{0.73}N$ optical waveguide layers coherently on AlN. The QDs were formed in the Stranski–Krastanov growth mode with a typical density in the 10^{11} cm^{-2} region [18]. They are hexagonal truncated pyramids with $\{1\bar{1}03\}$ facets. They have an average size (height/diameter) of about 2/10 nm, and nucleate on top of a wetting layer [19]. A 120 nm AlN cladding layer was grown on the top of the structure.

As regards the second heterostructure (figure 1) with quantum wells as the active medium (SCH–QW), it consisted of a 120 nm AlN layer first deposited on a GaN/sapphire Lumilog substrate [20], a 100 nm thick $Al_{0.5}Ga_{0.5}N$ epilayer, five GaN QW (1 nm thick) sandwiched between 8 nm thick $Al_{0.5}Ga_{0.5}N$ epilayers, the last $Al_{0.5}Ga_{0.5}N$ epilayer being 800 nm thick; on its top was grown a $Al_{0.25}Ga_{0.75}N$ epilayer 14 nm thick, a series of nine {1 nm thick GaN QW–8 nm thick $Al_{0.25}Ga_{0.75}N$ epilayers}, and a 14 nm thick $Al_{0.25}Ga_{0.75}N$ epilayer. Additionally, the structure was capped with a 100 nm thick AlN layer. The ELOG epilayer, which was 9 μm thick, was deposited on a (0001) sapphire substrate [21].

In situ plan-view CL experiments were performed at room temperature in a Hitachi 4700 cold field emission scanning electron microscope (FESEM) operating at 10 keV and equipped with a Gatan CL collecting mirror. A Jobin-Yvon H20 UV monochromator and a Perkin-Elmer photomultiplier were used to record the CL spectra. The beam current absorbed by the sample was varied in the range of 100 pA to about 2 nA. It was checked that the beam current to the absorbed current ratio, equal to 1.7 for all specimens, was constant; the beam current was measured with a Faraday cup. The time evolutions of monochromatic CL intensities were recorded while the electron beam was kept stationary for 30 min. It was always positioned outside dark defects and coalescence boundaries in the ELOG sample. When the monochromatic CL signal was too low to ensure a correct signal to noise ratio, the polychromatic intensity was recorded instead: this was the case for the SCH–QW and the ELOG specimens. The SCH–QD heterostructure was studied by recording either its polychromatic CL intensity, or the maximum intensity of the QD CL band. The CL images were analysed by means of home-made software.

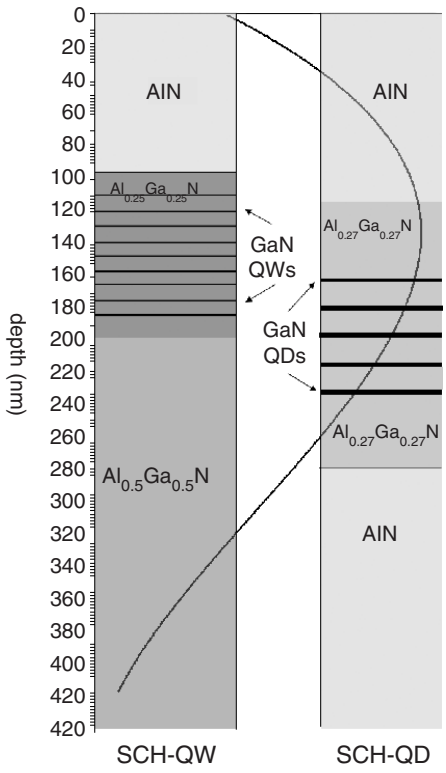

Figure 1. Schematic cross-sections of the SCH–QW and SCH–QD heterostructures. The curve symbolizes the normalized 10 keV depth–dose function which is the rate of energy dissipation per unit length per second [17].

3. Experimental results

3.1. CL spectra before electron beam irradiation

Figure 2(a) shows the CL spectra recorded in SCH–QD, SCH–QW and ELOG specimens before performing electron injection experiments. The minimum absorbed electron beam current enabling one to record a CL spectrum for the SCH–QW specimen was equal to about 1 nA because of the low CL efficiency of the GaN QW. The maximum of the GaN CL band for both SCH specimens occurs at a higher energy than that of the ELOG epilayer: 3.619 and 3.622 eV for the SCH–QD and SCH–QW specimens respectively, and 3.432 eV for the ELOG epilayer. The compressive strain in the latter being of the order of 1 GPa [22], the CL band is then blue shifted with respect to unstrained bulk GaN. Since the line shape is symmetrical, this means that the excess carrier density is smaller than 10^{19} cm^{-3} [23]. The GaN CL band of the ELOG specimen, which is attributed to the recombination of the free A exciton, is fitted with one Lorentzian (figure 2(b)); the lower energy shoulders correspond to the first and second phonon replicas [22]. The large full width at half-maximum (FWHM) of the CL GaN band observed for the SCH–QD specimen (220 meV) as compared to that for the SCH–QW one (140 meV) results from the QD size dispersion. The GaN and AlGaN CL bands of both specimens are well fitted with Gaussians (figure 2(c)) [16]. It is found that the CL intensity of the GaN QW band is about 40 times larger than that of the AlGaN CL

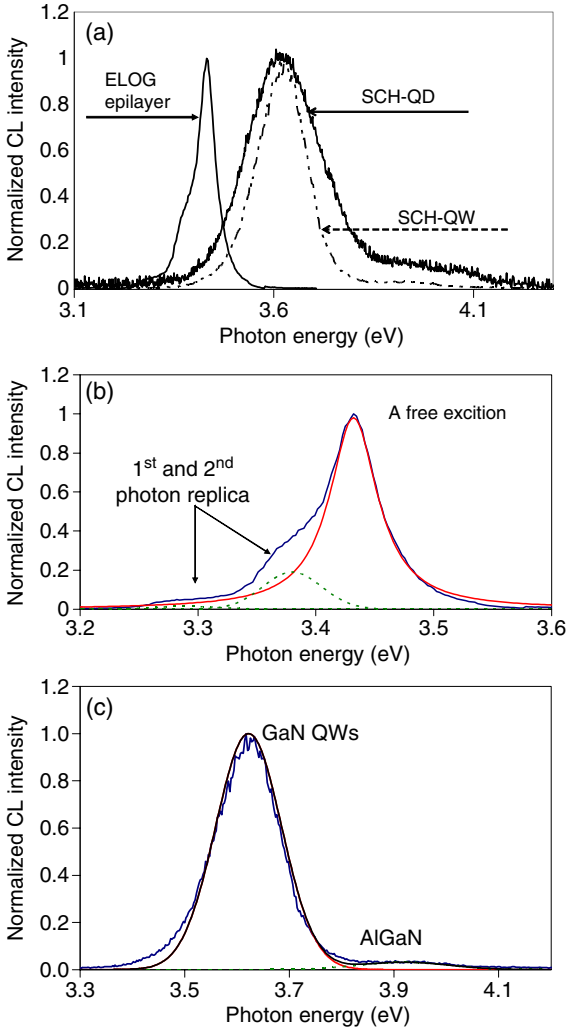

Figure 2. Plan-view normalized CL spectra recorded at room temperature on the ELOG epilayer and SCH–QD and SCH–QW specimens. The accelerating voltage is 10 kV, the absorbed beam current 1.6 nA. The spectra have been obtained in the TV mode on a 12 μm × 9.5 μm area. (a) Comparison of the ELOG epilayer and SCH–QD and SCH–QW specimens. (b) and (c) Deconvolutions of the CL spectra shown in figure 1(a). (b) Deconvolution of the ELOG epilayer CL spectrum shown in (a); the A exciton peak is fitted with a Lorentzian, and the first and second phonon replicas with a Gaussian (dashed curves), (c) Deconvolution of the SCH–QW CL spectrum shown in 2(a); the CL GaN QW band is fitted with a Gaussian, as is the AlGaN barrier. A similar fit has been found for the CL bands of the SCH–QD heterostructure [16].

band. Thus the polychromatic CL intensity recorded in the GaN QW heterostructure originates from the GaN QW only. The CL intensity of the GaN QD band is at least nine times larger than that of the AlGaN CL band. At an energy which corresponds to the maximum energy of the GaN QD band, the AlGaN barrier CL intensity is never larger than 1% of the GaN QD intensity. The fact that the UV CL band of the ELOG epilayer occurs at a lower energy than those of both SCH specimens is the first indication that the giant polarization induced electric field usually present in nitride-based semiconductors with the wurtzite structure [1] is

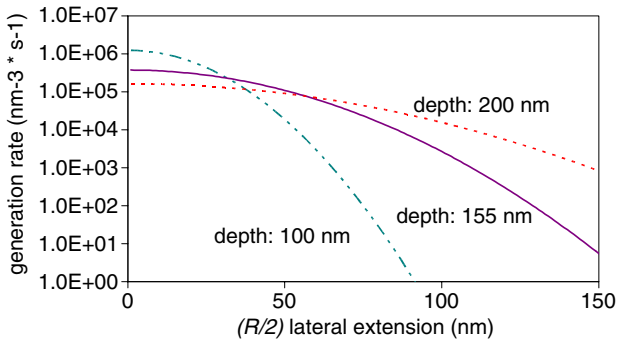

Figure 3. Lateral Gaussian extent of the pair generation rate per unit volume in three planes located at different depths below the free surface. The depths of 155 and 200 nm represent the mean depths of QWs and QDs respectively (figure 1). The 100 nm depth corresponds to the inverse of the absorption coefficient of the A exciton in the ELOG specimen. The 10 keV electron beam is located at $(R/2) = 0$. The calculations were performed with the expression given in [17].

screened by the excess carriers created by the electron beam. The second indication is given by the constant position of the GaN CL band of the SCH–QD and ELOG specimens when the absorbed electron beam current varies in the range of 0.24–1.6 nA. This could not be checked for the SCH–QW specimen due to its low CL efficiency. Nevertheless, we will assume flat band conditions for all three specimens.

3.2. 10 keV electron beam irradiation; comparison of luminescence properties of quantum dots, quantum wells and epilayers

The first important result of our study is that GaN and AlGaN epilayers, GaN QDs and QWs have identical behaviour as regards low energy electron beam irradiations. This means that, despite differences observed in their resistance to electron injection, epilayers, QWs and QDs have optical properties which are degraded in a similar way. More specifically, (i) the CL intensity decreases less rapidly with injection time when the beam current density increases, (ii) the surface of the area related beam injection increases with beam current density. Since these particular points have already been detailed for GaN QDs [16], we will focus in the present paper on the differences/similarities observed among the three specimens.

In the following the results are quoted in terms of absorbed beam current density J (A cm^{-2}) instead of absorbed beam current. As already noted in [15], the QD area concerned with the creation of electron–hole (e–h) pairs under beam injection has been estimated to have a value R of 200 nm, except when the absorbed beam current exceeds 3 nA. In that case, R, which again corresponds to the lateral extent of the e–h pair generation volume [15], is equal to about 300–350 nm.

The mean depth of the GaN QDs and QWs with respect to the specimen free surface has about the same value: 200 and 155 nm for GaN QD and GaN QW planes respectively. Calculations of the generation rate per unit volume ([17], figure 3) show that for identical electron beam operation conditions (beam current and accelerating voltage) a nearly identical lateral extent of the generation volume can be assumed in both QD and QW planes. As regards the ELOG specimen, one has to consider that the CL information depth is inversely proportional to the absorption coefficient α. In GaN, α is as large as 10^5 cm^{-1} for the free A exciton [24], so the information depth is about 100 nm. Thus, the lateral extent of the generation can, in

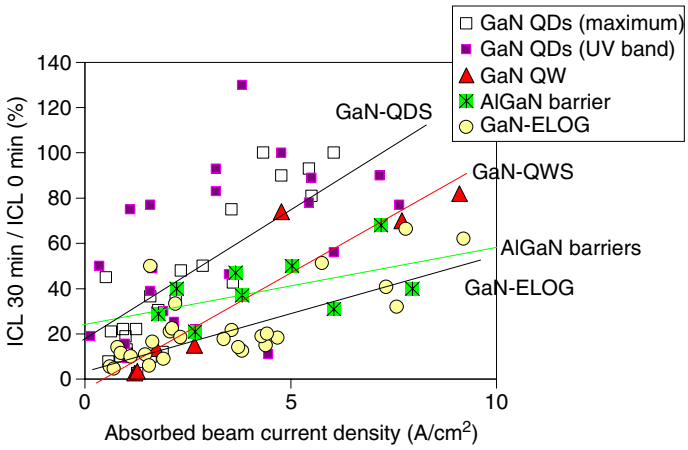

Figure 4. Variation of the I_{CL30}/I_{CL0} ratio with absorbed beam current density for the three specimens. I_{CL30} is the CL intensity remaining after 30 min of injection and I_{CL0} is its initial value. GaN QD (maximum) and GaN QD (UV band): the peak of the CL band and the polychromatic CL signal have been recorded respectively. The straight lines are guides for the eyes.

a first approximation, be taken equal to that in SCH specimens (figure 3). Therefore, the ratios of absorbed beam current density to absorbed beam current are nearly identical for all three specimens, allowing a direct comparison of their performance. The thickness d of the active layers which give rise to the CL signal is of the same order of magnitude for QDs and QWs, and it is much lower than that for the AlGaN epilayers and that for the ELOG specimen. This means that the beam current density injected in our experiments would be closer to the laser threshold current density J_{th} for the QD and QW heterostructures, since J_{th} is known to increase with d [25].

The level of resistance to e-beam injection of QDs, QWs and epilayers has been evaluated by plotting the I_{CL30}/I_{CL0} ratio with respect to the injected absorbed beam current density J; I_{CL30} is the CL intensity which remains after 30 min of beam injection, and I_{CL0} is the CL initial value.

The higher resistance of the GaN QDs is much more apparent at J values of >3–4 A cm^{-2} in the sense that the GaN QD I_{CL30}/I_{CL0} ratio is often as large as 100%, whereas that of GaN QWs and AlGaN and ELOG epilayers does not exceed 70–80% (figure 4). AlGaN barriers in SCH seem more resistant at low beam densities than is the ELOG epilayer. The opposite would be found at higher J values if the general tendency observed in figure 4 is a real one and is not due to a smaller amount of experimental results obtained on AlGaN barriers. The variations of the I_{CL30}/I_{CL0} ratio with J are nearly identical for GaN QWs and GaN QDs (figure 4); the GaN QW curve is simply shifted to lower I_{CL30}/I_{CL0} values with respect to the GaN QD curve. Thus it can be expected that a ratio of 1 could be obtained in QWs if J exceeded 10 A cm^{-2}. Several comparisons of the injection resistance of GaN QDs and AlGaN barriers performed on adjacent areas of the SCH–QD heterostructure indicate that at constant J value, the GaN dots are degraded less easily than the AlGaN barriers (figure 5). The scattering of the I_{CL30}/I_{CL0} ratio values seen in figure 4 for all specimens results from the spatial heterogeneity of their initial CL intensity [16]. For all specimens the time decrease of the CL intensity is fitted with either two independent exponential curves, as illustrated for AlGaN barriers and GaN QDs in figure 5(a), or sometimes by only one exponential curve. Usually, the first time decay τ_1 is smaller than the second one τ_2 (figure 5(a)). A noticeable feature is observed concerning

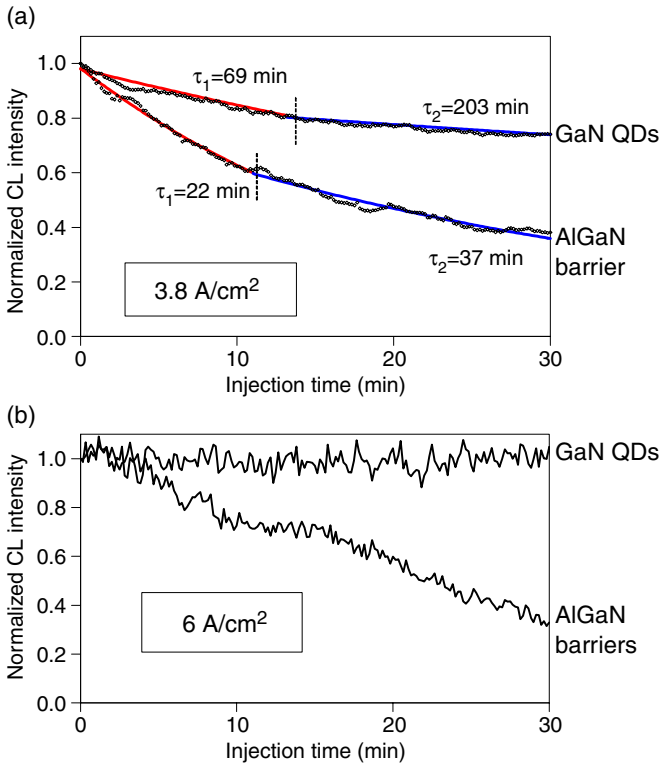

Figure 5. SCH–QD heterostructure. Normalized CL intensity as a function of beam injection time. GaN QDs are more resistant than AlGaN barriers at large absorbed beam current densities J. (a) $J = 3.8$ A cm^{-2}; the values of the exponential decay times which fit the curves are also shown (b) at $J = 6$ A cm^{-2}; the remaining CL intensity of GaN QDs after 30 min of beam injection can be as large as the initial one (see figure 4).

the mean value t_1 of the time interval of the first exponential decay: t_1 is of the order of few minutes in the ELOG epilayer and increases to about 15 min in GaN QDs and QWs (figure 6 (c)). In AlGaN barriers the CL decays have often been fitted with only one exponential; this means that, except at 4 A cm^{-2} (figure 6(a)), t_1 is larger in AlGaN barriers than in ELOG epilayers.

Figure 6 shows a compilation of the two time decay dependences on J for the three specimens. The results can be classified according to the J value:

(i) whatever the absorbed current density value J, the mean first and second time decays τ_1 and τ_2 are roughly largest in QDs and smallest in the ELOG epilayer, the difference being a little less significant in the case of τ_2 at low J,

(ii) at low J the same applies to the two mean values of τ_1 and τ_2 in QWs and QDs ($\tau_{1,\mathrm{QD}} > \tau_{1,\mathrm{QW}}$; $\tau_{2,\mathrm{QD}} > \tau_{2,\mathrm{QW}}$),

(iii) at large J, the mean time decays τ_1 and τ_2 in QDs and QWs are quite similar,

(iv) at low J, τ_1 and τ_2 in AlGaN barriers are smaller than those found in QDs,

(v) at large J, τ_1 values for AlGaN barriers are a little smaller than those for QWs, and significantly greater than those for the ELOG epilayer; τ_2 values for AlGaN barriers are a little smaller than those for QWs.

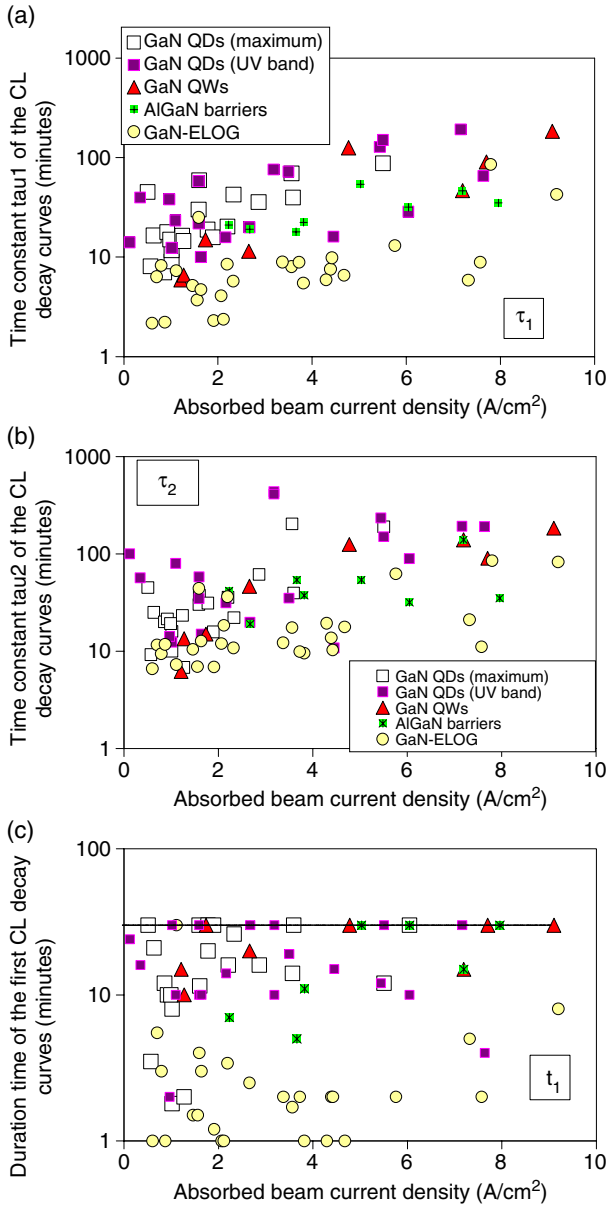

Figure 6. Comparison of the CL time decays τ_1 (a) and τ_2 (b) as a function of the absorbed current density J, in the three specimens studied: SCH–QD heterostructure (GaN QDs and AlGaN barriers) and SCH–QW heterostructure (GaN QWs). The mean time decays are really greater in GaN QDs, especially at low J. (c) Duration t_1 of the first CL decrease in all specimens. The dashed line corresponds to one unique time decay τ_1 equal to 30 min in our experiments.

All these results first strongly suggest that τ_1 and τ_2 do indeed correspond to two different mechanisms being involved in the degradation process, as already suggested in [15] and [16]. This point will be discussed further.

Since the time interval t_1 of the first exponential decrease varies from one area to another one in the same specimen, and also from one specimen to another, a plot of I_{CL} at different

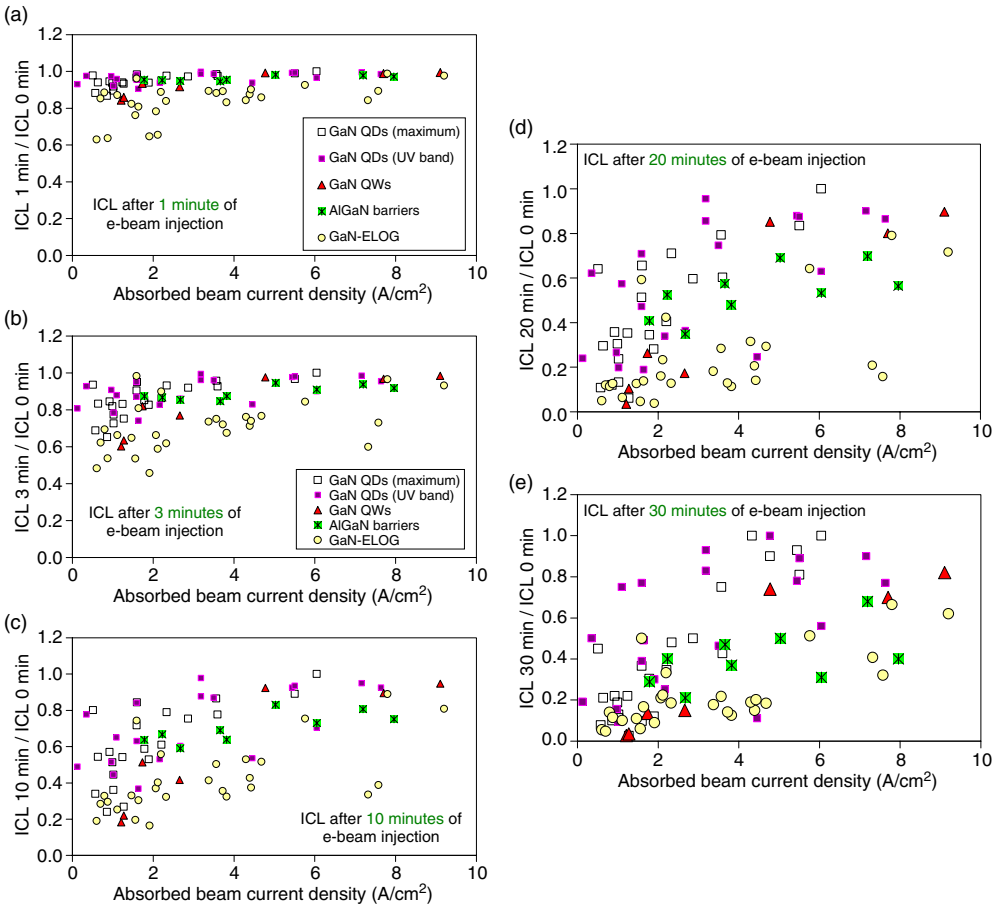

Figure 7. CL intensity in all specimens at various injection times t. The intensities are normalized with respect to the initial value I_{CL0}. (a) $t = 1$ min, (b) $t = 3$ min, (c) $t = 10$ min, (d) $t = 20$ min, (e) $t = 30$ min.

degradation times gives a better comparison between the epilayers, QDs and QWs. The CL intensities recorded after 1, 3, 10 and 20 min of e-beam injection are displayed in figure 7. During the first minute, the ELOG epilayer loses between 10 and 40% of its CL intensity (figure 7(a)). At low J values, the CL decrease is larger in GaN QWs, then in AlGaN barriers and finally in GaN QDs (figure 7). It has to be noted that the CL decrease in GaN QDs is far from being negligible at low J values: we observe a reduction of 10–50% (20–70%) during the first 3 (10) minutes. At large J values, the largest CL decrease is observed in the ELOG epilayer, then in the AlGaN barriers, then in the GaN QWs and finally in the GaN QDs (figure 7).

For all three specimens, dark spots or dark rings appear after e-beam injection (figure 8), depending on the J value. But, in contrast to what is observed for GaN QDs [16], GaN QWs and AlGaN barriers, no 'J rule' is observed for the ELOG epilayer (figure 9). The 'J rule' is as follows: when J is lower than about 1.5 A cm^{-2}, a dark spot appears whose centre is located at the injection point (figure 8(a)). When J is larger than 1.5 A cm^{-2}, a dark ring appears instead (figure 8(b)); the centre of the ring corresponds to the injection point. The 'J rule' and the value of 1.5 A cm^{-2} have been established from the results obtained for GaN QDs.

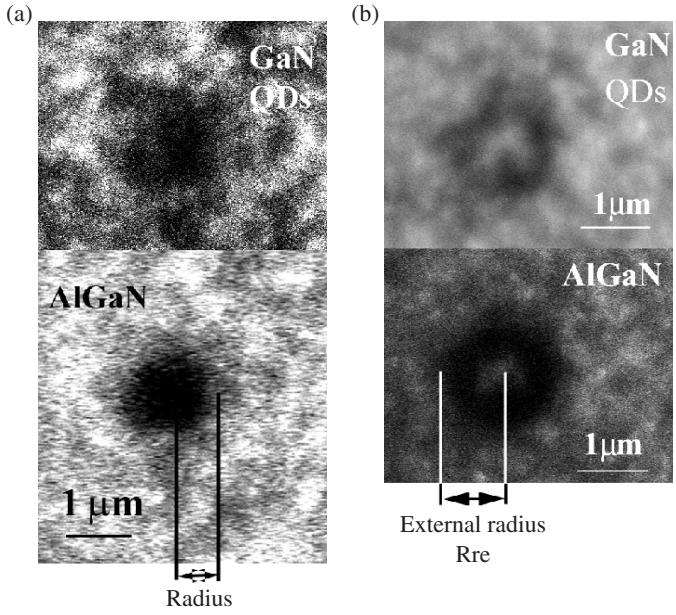

Figure 8. CL images of dark spots and dark rings which appear for all SCH heterostructures as well as ELOG epilayers after a 10 keV e-beam spot injection. (a) $J = 0.5$ A cm^{-2}. The dark ring radius can sometimes be larger for GaN than for AlGaN. (b) $J = 3.8$ A cm^{-2}. The external diameter of the dark ring is larger for AlGaN than for GaN QDs. Their shapes are frequently irregular for GaN QDs.

As shown in figure 9(b), a dark spot usually appears in ELOG specimens even after a beam injection larger than 1.5 A cm^{-2} with a radius quite independent of the J value. Furthermore, either a dark spot or a ring could be observed under injection at a constant current density (figure 9(b)). Dark spots and dark rings are, in the majority, the largest in AlGaN whatever the J value. One exception is shown in figure 8(a). The shape of the dark rings is often irregular in QDs owing to the microstructure (figure 8(b)). The latter, although also present in AlGaN barriers, does not influence the dark ring shape. At low J, dark spots are a little larger for QWs than for QDs, which is not the case for the dark rings observed at large J.

The last interesting result concerns the CL intensity profiles across the dark spots and dark rings. The CL profile of the very few dark spots for GaN QDs, AlGaN barriers and the ELOG epilayer has been found to be well fitted with a Gaussian (figure 10). No assessment can be made concerning GaN QWs since not many degradations were performed at low J values. Nearly all the dark spots have a flat CL profile such as those shown in figure 11. This is especially marked for the case of dark spots in the ELOG epilayers. As already noted, dark rings have been mainly observed in GaN QDs, GaN QWs and AlGaN barriers and not very often in ELOG epilayers. Their CL profile, shown in figure 12, seems to exhibit a kind of peak at the location of the injection point. This results from the fact that the e-beam spot was directed onto a 'bright' area such as those visible in figure 8.

4. Discussion

4.1. Decrease of the CL intensities

The decrease of the CL intensities could result from carbon contamination of the free surface. In such a case, a larger decrease should be observed when the beam current density increases

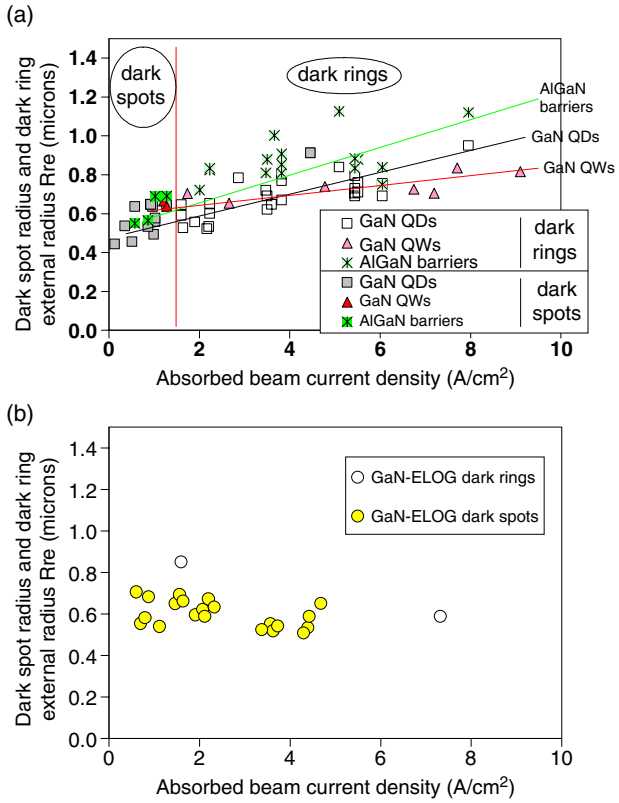

Figure 9. Dark spot radius and dark ring external radius R_{re} dependence on J. (a) SCH–QD and SCH–QW heterostructures. The 'J rule' is followed by GaN QDs and QWs as well as by AlGaN barriers. See the text for details. (b) ELOG epilayer. The 'J rule' is not followed. The lines are guides for the eyes.

since a thicker carbon film is expected to be deposited. Figure 4 for instance evidences that this is not the case. Therefore, this assumption can be ruled out.

The scatter of the experimental results in figures 4, 6, 7 and 9 shows that the specimen behaviour under e-beam irradiation is indeed a local property. For instance, an identical injected beam current density can lead to different values of the I_{CL30}/I_{CL0} ratio (figure 4), of the CL time decay times τ_1 and τ_2 (figure 6), as well as of the dark spot and dark ring radius (figure 9). Thus, the trends symbolized by the straight lines shown in figures 4 and 9(a) just show that the resistance of the specimens increases with the beam current density and give a rough indication of the general degradation behaviours. As will be detailed in the following, the degradation of all the specimens we have studied is promoted by the presence of NR centres. Therefore, the spatial fluctuation of their density within one specimen leads to the spatial variation of its degradation properties. Actually the differences in QD, QW and epilayer strength of resistance to e-beam injection arise from the ability of excess carriers to experience more or fewer NR recombinations; but, as will be demonstrated, the underlying mechanisms of degradation are similar for all the specimens that we have studied.

4.2. Formation of dark spots

It appears that the formation of dark spots at low J in quantum dots, quantum wells and epilayers exposed to low energy e-beam injection occurs via two similar serial mechanisms

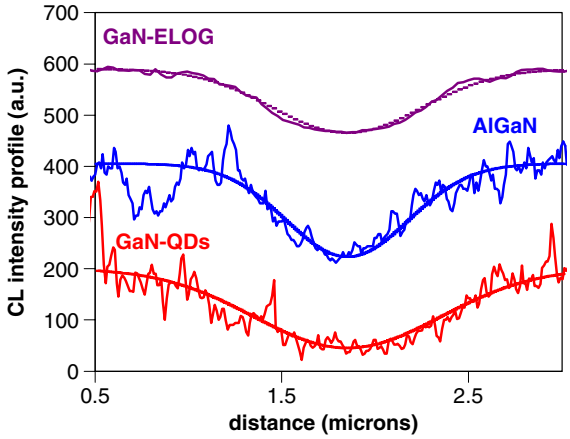

Figure 10. Gaussian CL profiles across dark spots. The dark spots for GaN QDs and AlGaN barriers were recorded after an e-beam injection at 0.5 A cm^{-2} (figure 6(a)), as was the dark spot for the ELOG epilayer. All the CL profiles are Gaussian.

which form the model of recombination enhanced diffusion of defects. From our experimental results, we can detail this model a little more [5]. In the first place, charge carriers created by the electron beam diffuse outside the generation volume, and undergo NR recombinations induced by the presence of initially present NR centres, whose density is called N_{NR0}. These NR recombinations and/or UV photons are able to break complexes of density N_{NR1} already present in the specimens such as those formed with gallium vacancies V_{Ga} and impurities (V_{Ga}–Si_{Ga}, V_{Ga}–O_N for instance). Free vacancies V_{Ga} of density N_{NR1} could then be liberated, undergo diffusion within the specimens and form aggregates or dislocation loops which are known to be able to release strain and induce a decrease of the luminescence signal [26]. Actually, NR recombinations in SCH–QD and SCH–QW heterostructures can occur at dislocations which have been found at quite large density—3×10^{10} cm^{-2} in the SCH–QD heterostructure [27]—and which are known to act as NR recombination centres [22, 28, 29]. Dislocations, which are arranged in low angle grain boundaries leading to a mosaic and columnar structure, are therefore present in the AlGaN barriers of the SCH–QD heterostructure. Furthermore, threading edge dislocations being effective nucleation sites for quantum dots [30], efficient NR recombinations can occur close to the dots. This could explain why the GaN QDs studied here are not as resistant to e-beam injection as could have been expected.

The time decay τ_1 of the CL intensity depends on both N_{NR0} and N_{NR1}, the initial and the recombination enhanced diffused NR centre (RED centre) densities respectively, but also on the minority charge carrier diffusion length L. The larger the value of L, the greater the number of available NR recombination centres, and the faster the CL decrease. This accounts for the greater resistance, during the first minutes of irradiation, of the quantum dots where the charge carriers are three-dimensionally (3D) confined (figure 7). Comparison of τ_1 values in figure 6(a), which yields $\tau_{1,GaN-QD} >= \tau_{1,AlGaN} > \tau_{1,GaN-QW} > \tau_{1,GaN-ELOG}$, then shows that even if the total NR centre densities are similar, as we think is the case for SCH–QD and SCH–QW heterostructures, the diffusion length value is a very important parameter in the degradation process, as already stated. The smaller τ_1 value observed for the ELOG epilayer can result from a larger NR centre density. Moreover, since charge carriers can diffuse more easily in quantum wells, they degrade quite similarly to ELOG epilayers (figure 7).

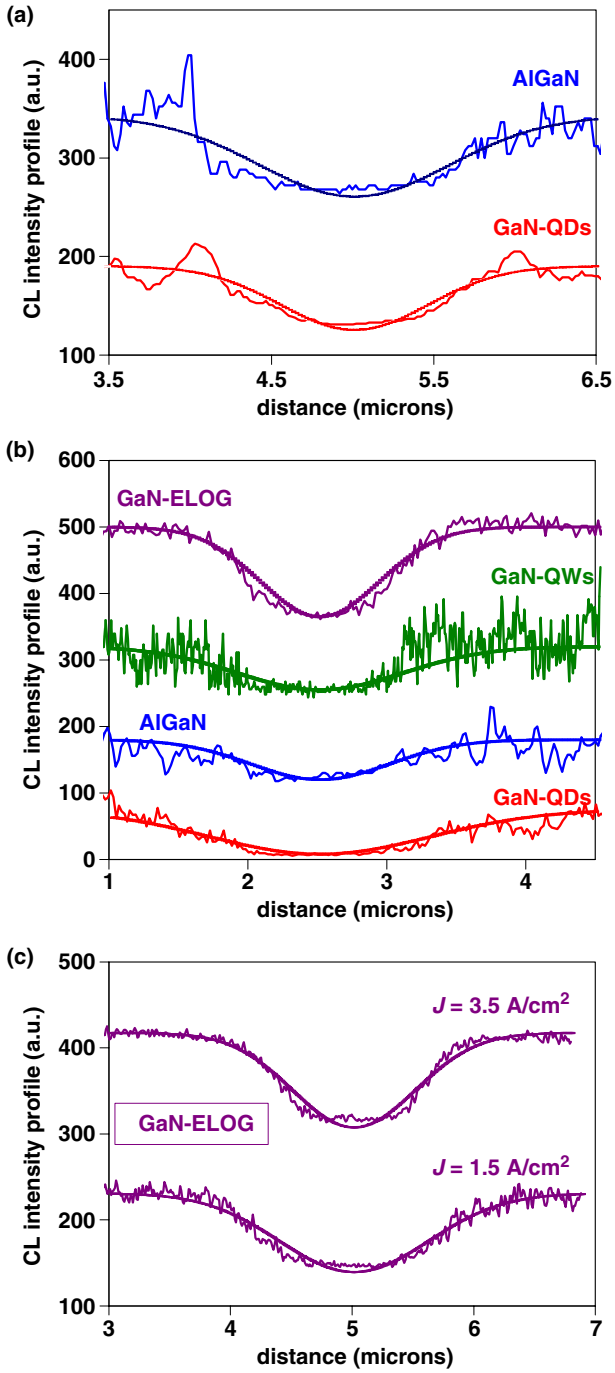

Figure 11. Examples of nearly or non-Gaussian experimental CL profiles across dark spots for both heterostructures and epilayers. Spotty lines show the best Gaussian fits of experimental CL profiles. (a) The AlGaN barrier CL profile is larger and flatter than the GaN QD one. $J = 0.86$ A cm^{-2}. (b) The AlGaN profile is nearly Gaussian whereas the GaN one, like those recorded for the GaN QWs and the ELOG specimen, is not. $J = 1.27$ A cm^{-2}. (c) The examples shown here are representative of CL profiles across dark spots for the ELOG specimen.

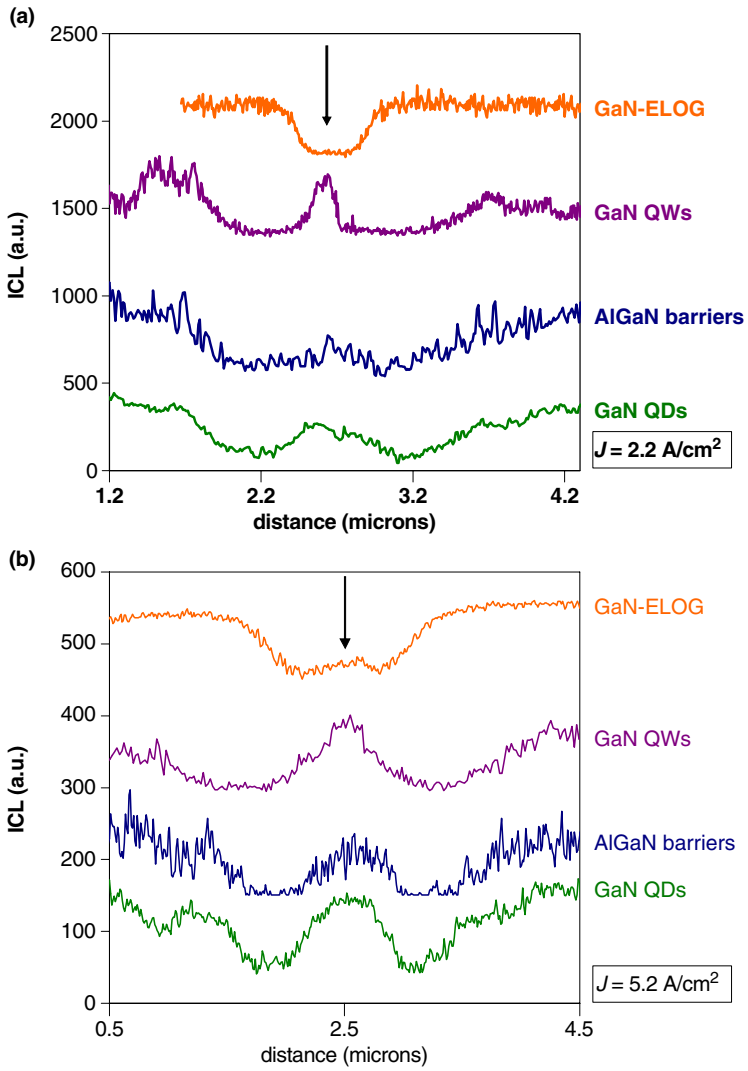

Figure 12. CL profiles across dark rings for SCH heterostructures and epilayers for two different beam current densities. The arrows indicate the injection points. (a) $J = 2.2$ A cm^{-2}. The CL profile across a dark spot for the ELOG epilayer is shown as a reference. (b) $J = 5.2$ A cm^{-2}.

The time duration t_1 of the first exponential CL decrease seems to depend on N_{NR1}, the density of RED centres necessary to start forming dislocation loops whose multiplication and development could constitute the mechanism responsible for the second CL exponential decay. The smallest value of t_1 being for the ELOG epilayer confirms the presence of a larger N_{NR0} value for the initial NR centre density within this epilayer.

The lateral profile of the excess carriers generated is known to be Gaussian [17]. Thus, the systematic occurrence of a non-Gaussian CL profile across the dark spots in all specimens evidences the occurrence of a recombination enhanced diffusion of NR defects during e-beam injection. This diffusion, which tends to equalize the CL intensity, and therefore the total NR centre density, is faster when the absorbed beam current density J is greater than 0.5 A cm^{-2}.

Our results show that the degradation behaviour of AlGaN barriers is closer to that of GaN QDs, whereas a similarity with the ELOG epilayer was expected. In fact, the only similarity is found among all specimens in the dark spot radius value at low J (figure 9). The AlGaN/GaN QDs similarity could result first from a kind of interaction between them in the sense that carriers can move from one to the other. Actually, the lateral extent of the dark spots and specifically of the dark rings demonstrates that carrier migration in the QD planes is far from being negligible (figures 8,10 and 11). Indeed carriers created in the AlGaN barriers can be captured by the potential wells formed by the dots. Further, the motion of carriers can be assisted by tunnelling between the dots, or by their thermal emission from one dot followed by recapture into neighbouring QDs [31].

Second, as it has been mentioned previously, the N_{NR0} centre densities should be similar in AlGaN barriers and GaN QDs, since they both constitute an SCH–QD heterostructure. Thus the number of available NR recombinations in AlGaN layers is certainly closer to that in GaN QDs than to that in the ELOG epilayer. The larger value of dark spot radii observed for AlGaN, in the majority, compared to those for GaN QDs (figures 9(a) and 11(a)) could be due to an increased migration of carriers and/or of NR centres along AlGaN layers as compared to that along GaN QD ones. The lateral migration of carriers in both AlGaN and QDs layers could also be enhanced by photon reabsorption which is known to be efficient in semiconductors with a high absorption coefficient value.

4.3. Formation of dark rings

When J increases, the CL intensity decrease at the injection point becomes less important, and the dots get more and more resistant as compared with quantum wells and epilayers (figures 6 and 7). At large J values (>1.5 A cm^{-2}), dark rings appear instead of dark spots (figures 8(b), 9 and 12) for SCH–QD and SCH–QW heterostructures. This occurs when the injected current density is large enough to saturate the initial NR recombination centre density [16]. The CL degradation should follow the same schematic model as in the 'low J' case, but with a longer time constant. Excess carriers move along the QD layers a larger distance until they reach a density such that NR recombinations become, as in the 'low J' case, more efficient than radiative recombinations. Thus, the process which lies at the origin of the dark spot formation can start again, and a dark ring appears (figure 8(b)). A much larger density of initial NR centres in the ELOG specimen accounts for the fact that very few dark rings were produced by e-beam injection (figure 9(b)).

As expected, the resistances of AlGaN and ELOG epilayers are similar at large J values (figure 7), since they arise from the greater possibility of excess carriers moving freely in epilayers, as compared with the confined systems case, and then undergoing NR recombinations. This also explains the larger dark ring value R_{re} for AlGaN compared with GaN QDs (figure 9(a)). At large J values, the behaviour of GaN QWs seems to tend towards that of GaN QDs and less to that of epilayers (figure 7). This behaviour is unexpected, since the excess carriers are 3D confined in quantum dots whereas they can diffuse in QWs. Two reasons can be evoked to explain that particular point:

(i) the GaN QDs are connected with AlGaN barriers in terms of excess carrier motion as already noted and one can still consider the possibility of thermal emission of excess carriers from one dot, their diffusion in the barrier and their recapture into neighbouring QDs [31];
(ii) the saturation of initial NR centres leads to an increase of the recombination time [16], but the diffusion of excess carriers in the QW planes decreases with J since the mobility is reduced by efficient carrier–carrier scattering [32].

This accounts for the slower augmentation of the dark ring value R_{re} for QDs compared with AlGaN barriers and QDs (figure 9(a)). As regards the ELOG epilayer, the J value was not large enough for saturation of the initial NR centres, particularly since no dislocations were present in the areas where injection experiments were performed.

5. Conclusion

In situ cathodoluminescence experiments were performed on GaN quantum wells and quantum dots as well as ELOG and AlGaN epilayers to study their room temperature resistance to 10 keV electron irradiation. It was shown that the higher resistance of the dots was much more apparent when the beam current density was larger than about 6 A cm^{-2}. For all specimens the CL signal decays with time and can be fitted with two independent exponential curves. This evidences that the model of recombination enhanced diffusion of defects is general and that it relates to the degradation of quantum dots, quantum wells and epilayers. The presence of a large density of non-radiative centres in a specimen leads not only to an increase of the laser threshold current density J_{th}, but also to a faster degradation of the specimen luminescence properties.

NR recombinations promote degradation of the CL signal by enhancing the diffusion of point defects (first mechanism) which can agglomerate to form dislocation loops (second mechanism). The very beginning (first minutes) of the degradation is the most important since the resulting CL intensity is mainly dependent on the time decay of the first exponential decrease as well as on its duration. One could expect to increase the resistance of the specimens to e-beam injection, specifically that of quantum dots, by reducing the dislocations and the initial point defect densities. At large injection, the resistance of quantum wells becomes more similar to that of quantum dots than to that of epilayers since the diffusion of excess carriers is almost constant with injection.

Acknowledgments

The author would like to thank C Vanmansart for his active participation in the CL experiments as well as for the CL image software. J Barjon (CNRS-Meudon), E Monroy and B Daudin (CEA-Grenoble) are gratefully acknowledged for the SCH–QD and SCH–QW heterostructures, as are B Beaumont (Lumilog) and P Gibart (CRHEA-CNRS) for the ELOG epilayer. This work was partly supported by the TIPEL project (DiG-ITIP 3/STSI/SDCO).

References

[1] Morkoç H, Neogi A and Kuball M 2004 *Fall MRS 2003*; *Mater. Res. Soc. Symp. Proc.* **789** N 8.5 and references therein
[2] Gérard J M, Cabrol O and Sermage B 1996 *Appl. Phys. Lett.* **68** 3124
[3] Dassonneville S, Amokrane A, Sieber B, Farvacque J-L, Beaumont B, Gibart P, Ganière J-D and Leifer K 2001 *J. Appl. Phys.* **89** 7966
[4] Haberer E D, Chen C H, Hansen M, Keller S, DenBaars S P, Mishra U K and Hu E L 2001 *J. Vac. Sci. Technol.* B **19** 603
[5] Mera Y, Suzuki K and Maeda K 2003 *Physica* B **340–342** 488
[6] Sobolev N A, Cavacon A, Carmo M C, Grudmann M, Heinrichsdorff F and Bimberg D 2001 *Phys. Status Solidi* b **224** 93
[7] Leon R, Swift G M, Magness B, Taylor W A, Tang Y S, Wang K L, Dowd P and Zhang Y H 2000 *Appl. Phys. Lett.* **76** 2074
[8] Marcinkevicius S, Siegert J, Leon R, Cechavicius B, Magness B, Taylor W and Lobo C 2002 *Phys. Rev.* B **66** 235314
[9] Ribbat Ch, Sellin R, Grundmann M, Bimberg D, Sobolev N A and Carmo M C 2001 *Electron. Lett.* **37** 174

[10] Schoenfeld W V, Chen C-H, Petroff P M and Hu E L 1998 *Appl. Phys. Lett.* **73** 2935
[11] Piva P G, Goldberg R D, Mitchell I V, Labrie D, Leon R, Charbonneau S, Wasilewski Z R and Fafard S 2000 *Appl. Phys. Lett.* **77** 624
[12] Ota T, Maehashi K, Nakashima H, Oto K and Murase K 2001 *Phys. Status Solidi* b **224** 169
[13] Rodriguez-Viejo J, Mattoussi H, Heine J R, Kuno M K, Michel J, Bawendi M G and Jensen K F 2000 *J. Appl. Phys.* **87** 8526
[14] Lundina E Y, Shernyakov Y M, Maksimov M V, Kayander I N, Tsatsul'nikov A F, Ledentsov N N, Zhukiv A E, Maleev N A, Mikhrin S S, Ustinov V M, Alferov Zh I and Bimberg D 2003 *Techn. Phys.* **48** 131
[15] Verbert J, Barjon J, Monroy E, Daudin B and Sieber B 2004 *J. Phys.: Condens. Matter* **16** S243
[16] Sieber B 2005 *J. Appl. Phys.* **98** 083250
[17] Donolato C 1981 *Phys. Status Solidi* a **65** 649
[18] Daudin B, Widmann F, Feuillet G, Samson Y, Arlery M and Rouvière J L 1997 *Phys. Rev.* B **56** R7069
[19] Gogneau N, Enjalbert F, Fossard F, Hori Y, Adelmann C, Brault J, Martinez-Guerrero E, Simon J, Bellet-Amalric E, Jalabert D, Pelekanos N, Rouvière J-L, Daudin B, Dang S L, Mariette H and Monroy E 2004 *Phys. Status Solidi* c **1** 1445
[20] http://www.lumilog.com/
[21] Beaumont B, Bousquet V, Vennéguès P, Vaille M, Bouillé A, Gibart P, Dassonneville S, Amokrane A and Sieber B 1999 *Phys. Status Solidi* a **176** 567
[22] Dassonneville S, Amokrane A, Sieber B, Farvacque J-L, Beaumont B and Gibart P 2001 *J. Appl. Phys.* **89** 3736
[23] Leroux M, Beaumont B, Grandjean N, Lorenzini P, Haffouz S, Vennéguès P, Massies J and Gibart P 1997 *Mater. Sci. Eng.* B **50** 97
[24] Muth J F, Lee J H, Shmagin I K, Kolbas R M, Casey H C Jr, Keller B P, Moshra U K and DenBaars S P 1997 *Appl. Phys. Lett.* **71** 2572
[25] Kapon E (ed) 1999 *Semiconductors Lasers I Fundamentals* (New York: Academic)
[26] Bonard J M, Ganière J-D, Vanzetti L, Paggel J J, Sorba L, Franciosi A, Hervé D and Molva E 1998 *J. Appl. Phys.* **84** 1263
[27] Barjon J, Brault J, Daudin B, Jalabert D and Sieber B 2003 *J. Appl. Phys.* **94** 2755
[28] Rosner S J, Carr E C, Ludowise M J, Girolami G and Erikson H I 1997 *Appl. Phys. Lett.* **70** 420
[29] Sugahara T *et al* 1998 *Japan. J. Appl. Phys.* 2 **37** L398
[30] Rouvière J L, Simon J, Pelekanos N, Daudin B and Feuillet G 1999 *Appl. Phys. Lett.* **75** 2632
[31] Lobo C, Lean R, Marcinkevicius S, Yang W, Sercel P C, Liao W Z, Zou J and Cockayne D J H 1999 *Phys. Rev.* B **60** 16647
[32] Carosella F, Germain M and Farvacque J-L 2005 *Fall MRS 2004*; *Mater. Res. Soc. Symp. Proc.* **831** E8.6.1